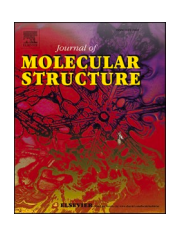
ELSEVIER

Contents lists available at ScienceDirect

Journal of Molecular Structure

journal homepage: www.elsevier.com/locate/molstr





A new Thiadiazole-triazine derivative: Structural investigation, DFT studies, ADME-T analysis and SARS-CoV-2 activity by docking simulation

Lohith T. N. ^{a,e}, Chandra ^{a,*}, Gayathri B. H. ^{b,*}, Shamantha Kumar ^c, Shivaprasad C. M. ^d, Divya K. ^b, Sridhar M. A. ^e, Mahendra M. ^e

- ^a Department of Physics, The National Institute of Engineering, Mysuru 570008, Karnataka, India
- ^b PG Department of Chemistry, BMS College for Women, Basavanagudi, Bangalore 560004, Karnataka, India
- ^c Department of Physics, SJB Institute of Technology, Bengaluru 560060, Karnataka, India
- ^d Department of Chemistry, Government Science College, Hassan, Karnataka 573201, India
- e Department of Studies in Physics, University of Mysore, Manasagangotri, Mysuru 570 006, Karnataka, India

ARTICLE INFO

Keywords: Thiadiazole-triazine derivative Crystal structure DFT HOMO-LUMO Omicron variant of SARS-CoV-2 spike protein

ABSTRACT

The present work involves the synthesis of thiadiazole-triazine derivative 7-[2-(4-bromophenyl)ethenyl]-3-tert-butyl-4H-[1,3,4]thiadiazolo[2,3-c][1,2,4]triazin-4-one (TCA3) and spectroscopic characterization is done using NMR and X-ray diffraction techniques. The single crystal X-ray diffraction study unravels the 3D structure of the compound TCA3. The compound crystallizes in the monoclinic crystal system with the space group P2₁/c. The crystal structure analysis revealed that various C—H...O, C—H...N, and C—H...Br interactions are responsible for crystal packing. Furthermore, Hirshfeld surface analysis has been performed to visualize and analyze the intermolecular interactions observed in the crystal structure. Energy framework analysis was used to explore the molecular architecture in the crystal, and to calculate the molecular interaction energies of the compound TCA3. DFT calculations have also been carried out to explore the various physicochemical properties of the compound like HOMO-LUMO energy gap of the molecule, reactive sites present in the molecule using MEP analysis. The energy gap of the molecule is found to be 4.592 eV. Also, to know the strength and nature of intramolecular interaction energy using RDG analysis. Finally, the potential inhibitory activity of the titled compounds and their drug-likeness are demonstrated by ADME-T calculations. Further, The structure-activity relationships established through molecular docking studies showed that the compound TCA3 strongly binds to the receptors Mpro (-8.2 Kcal/mol) which confirm its inhibition activity against COVID-19.

1. Introduction

Triazines and their derivatives are significant classes of heterocyclic compounds. These compounds are highly sought after for their anticancer, anti-HIV, antiviral, antimalarial, antibacterial, antifungal, and antioxidant properties [1]. Triazines are widely used as herbicides [2] and insecticides [3] in agriculture. Thiadiazole compounds with the –NCS moiety demonstrate diverse biological activity [4]. Bartlett et al. identified 1,2,4-triazinones as anti-inflammatory drugs with immune modifying characteristics [5]. Researchers found that these chemicals effectively prevent and treat arthritic diseases in rats. These compounds decreased carrageenan-induced paw edema, attenuated the active Arthus response, and showed antierythema and antipyretic effects [6]. A useful strategy in drug development is combining two or more

pharmacophoric scaffolds to produce new hybrid molecules that may have increased affinity and efficacy [7]. There are currently no effective anti-coronavirus drugs available. Several medicines, including Hydroxychloroquine and Remdesivir, are being evaluated in clinical studies for their efficacy in treating COVID-19 patients. A recent study found that Remdesivir and Chloroquine inhibit the growth of SARS-CoV-2 in vitro [8–14]. Remdesivir has demonstrated significant activity against SARS-CoV-2 both in vitro and in animal, and clinical trials are under underway. Computational studies are performed to investigate the structure, stability, and potential binding mechanisms and interactions of ligands with the enzyme site. The physicochemical and electrical properties of medicinal molecules can impact their chemical and biological activities. Quantum chemical simulations utilizing Density Functional Theory (DFT) are commonly used to identify drug active sites

E-mail addresses: chandru@nie.ac.in (Chandra), gayathribh14@gmail.com (G. B. H.).

^{*} Corresponding authors.

and correlate activity with various factors [15–17]. DFT calculations can be used to investigate various biological activities of bioactive compounds. In continuation of our efforts in the search for novel anti-viral agents, we report the synthesis and structural investigation of 1,3,4-thiadiazole-triazine hybrids (TCA3). In this study, we have synthesized and characterized a series of 1,3,4-thiadiazole-triazine hybrids using different spectroscopic techniques. The synthesized triazine-thiadiazole hybrids were also analyzed via DFT and docking analysis for their activity performance to get insight into the interactions and binding modes in the active site of this enzyme. Triazine-thiadiazole ring scaffolds have been used to synthesize novel anti-COVID drugs with numerous reaction sites, allowing for diverse therapeutic applications [18]. There are currently no appropriate antiviral medications for treating COVID-19. Redesigning existing drugs can be an effective treatment technique. Despite FDA-approved medications like lopinavir, remdesivir, and chloroquine [19], the search for an effective drug continues.

2. Methods and materials

The chemicals 3,3-dimethyl-2-oxobutanoic acid, hydrazine hydrate, carbondisulfide, phenylacetic acids and phosphorus oxychloride used for the synthesis of novel thiadiazolotriazin-4-ones were procured from Sigma-Aldrich, Bengaluru, India. Melting points of the compound (5) were determined in open capillary tubes and were uncorrected. The purity of the synthesized compounds was checked by TLC, showing a single spot on Merck silica gel 60 F254 coated alumina plates. The structure of TCA3 was confirmed by spectral studies. The ¹HNMR and ^{13C}NMR spectra were recorded on a Bruker AMX-400 (400, 100 MHz, respectively) spectrometer using DMSO-d6 as solvent and TMS as the internal standard. The Mass spectra were recorded on PerkinElmer 018,444–Y, Triple Quadrupole LC/MS Spectrometer.

2.1. Synthesis and characterizations

2.1.1. General procedure for the synthesis of 4-Amino-6-Tert-Butyl-3-Sulfanyl-1,2,4-Triazin5(4 h)-One (3)

thiocarbohydrazide (1) (5.3 g, 0.05 mol) and 3,3-dimethyl-2-oxobutanoic acid (trimethyl pyruvic acid) (2) (6.5 g, 0.05 mol) were refluxed in ethanol for 10 h. The completion of the reaction and purity was monitored by running thin layer chromatography in ethyl acetate and petroleum ether mixture. After 10 h, the reaction mixture was poured into crushed ice. The solid product obtained was filtered under vacuum using ethanol. The schematic representation is given in Scheme 1.

2.1.2. General procedure for the synthesis of 7-[2-(4-bromophenyl) ethenyl]—3-tert-butyl-4H-[1,3,4]thiadiazolo[2,3-c][1,2,4]triazin-4-one (TCA3)

4-amino-6-tert-butyl-3-sulfanyl-1,2,4-triazin-5(4H)-one(3) (0.005 mol) and 4-Bromo Cinnamic acid (4) (0.005 mol) were condensed in $POCl_3$ at $90^{\circ}C$ for 10 h. The reactions were carried out in dry condition. The reaction mixture was substituted then cooled, and the solid product was separated by pouring the reaction mixture into crushed ice. The solid product obtained was filtered, washed, dried from ethanol. The schematic representation of the synthesis of the final compound **TCA3** is given in Scheme 2. The crystals are grown using a slow evaporation

Scheme 1. Synthetic pathway of the compound (3).

method using ethanol as a solvent at ambient temperature.

2.1.3. Spectral characterizations

IR(cm⁻¹): 2964 (C—H, 4-bromo phenyl moiety), 2923 (C—H, *tert* butyl moiety), 1693 (C = O), 1624 (C = N-), 1510 and 1361 (C = C), 1457 (N—N), 1262 (C-S-), 814 (C-Br). ^{1H}NMR (DMSO, δ ppm): 1.42 (9H, s, *tert* butyl groups), 7.78 (2H, d, J=8.4 Hz, 4-Br phenyl ring), 7.67–7.69 (4H, m, 4-Br phenyl ring and HC—CH). ^{13C}NMR (δ ppm): 28.0 (3C *tert* butyl moiety), 37.9 (quaternary \underline{C} atom, of *tert* butyl moiety), 118.4 (ethylene \underline{C} atom), 124.4, 130.6, 132.2, 132.4, 134.0, (2C atoms of 4-Bromo Phenyl ring), 142.4 (ethylene \underline{C} atom) 147.2, 159.7, 159.5 (3C atoms thiadiazolotriazin-4-one) and 160.60 (>C = O, thiadiazolotriazin-4-one). LC-Mass [M+], (m/z): 389.9/394.0. The Mass, ^{1H}NMR, ^{13C}NMR, and FT-IR spectra are given in supplementary file as figure S1-S4 respectively.

2.2. X-ray crystallography

A good quality suitable crystals were selected for the X-ray intensity data collection using Bruker Venture diffractometer equipped with the MoKa radiation (λ =0.71073 Å) at room temperature 293 K. The data were collected and processed using SAINT SADBS software. The structure was solved by utilizing the direct methods with the help of SHELXS and refined against F^2 with full-matrix least-squares using SHELXL-2019/3 [20,21]. All hydrogen atoms were placed at calculated positions and allowed to ride on their parent atoms. Non-hydrogen atoms were refined anisotropically. The crystal and refinement details are provided in the Table 1. The geometrical calculations were carried out using PLATON software [22]. The publication quality images like ORTEP packing diagrams were generated using Mercury [23].

2.3. Computational studies

The Hirshfeld surface analysis and decomposed 2D fingerprint plots were carried out to understand the various non-covalent interactions involved in the compound TCA3 using the software CrystalExplorer 17.5 [24]. For energy frameworks calculation, the B3LYP/6–31G(d,p) level of theory was used as recommended by the CrystalExplorer program. The gas phase structural optimization and vibrational frequency calculation were carried out using the program Gaussian09 [25] with the Minnesota functional ω B97X basis set was used along with the Grimme's empirical dispersion (D3) correction [26]. The vibrational frequency calculation revealed that no imaginary frequency was found, which in turn confirmed true energy minima on the potential energy surface. Further, the reduced density gradient analysis have been carried out to understand the strength and nature of weak interactions present in the compound TCA3 using Multiwfn software [27]. The results were visualized by Visual Molecular Dynamics (VMD) software [28].

2.4. in-silico studies

2.4.1. ADME-T profile

The understanding of the behaviour of the synthesized compound with the human body is crucial in proceeding towards the development of the drug. Hence, to explore the pharmacokinetic properties such as absorption, distribution, metabolism, excretion, and toxicity of the compound ADMET analysis was carried out using SwissADME and pkCSM server. Further, other properties of the compound such as hydrophilicity, hydrophobicity, solvent accessible surface area, number of rotatable bonds, donor-hydrogen bonds, acceptor-hydrogen bonds, blood brain barrier permeability (BBB), Caco-2 cell permeability, human intestinal absorption (HIA). Skin permeability, cytochrome P450 2D6 binding (CYP2D6), hepatotoxicity and plasma protein binding (PPB) were explored. These properties play a major role in the drug development.

Scheme 2. Synthetic pathway of the compound (TCA3).

Table 1Crystal data and structure refinement details.

Parameters	Values
CCDC Number	1,525,567
Empirical formula	$C_{16}H_{15}BrN_4OS$
Formula weight	391.28
Temperature	293 K
Wavelength	0.71075 Å
Reflns. for cell determination	15,801
θ range for above	3.32° to 27.49°
Crystal system	Monoclinic
Space group	P 2 ₁ /c
Cell dimensions	a = 13.099(2) Å
	b = 12.1114(19) Å
	c = 11.3616(17) Å
	$lpha=90^\circ$
	$\beta=110.310(8)^\circ$
	$\gamma=90^\circ$
Volume	1690.4(5) Å ³
Z	4
Density(calculated)	$1.538 \; \mathrm{Mg} \; m^{-3}$
Absorption coefficient	2.564 mm^{-1}
F_{000}	792
Crystal size	0.250 × 0.250 × 0.250 mm
θ range for data collection	3.32° to 27.49°
Index ranges	$-16 \le h \le 16$
	$-15 \le k \le 15$
	$-14 \leq l \leq 14$
Reflections collected	15,801
Independent reflections	$3827 [R_{int} = 0.115]$
Absorption correction	Multi-scan
Refinement method	full matrix least-squares on F^2
Data / restraints / parameters	3827 / 0 / 221
Goodness-of-fit on F^2	1.012
Final R indices $[I > 2 \sigma(I)]$	R1 = 0.0903, wR2 = 0.1851
R indices (all data)	R1 = 0.2213, wR2 = 0.2353
Largest diff. peak and hole	0.855; −0.332 e Å ^{−3}

2.4.2. Molecular docking analysis

Molecular docking is a versatile computational technique used to predict the binding affinity of the synthesized compound with the proteins. The 3D structure of the SARS-CoV-2 omicron spike protein (PDB ID: 7WWK) [29] were downloaded from the protein data bank in pdb format. The water molecules and the ligand associated with the protein was removed using Autodock MGL 1.5.6 tools [30,31]. Further, polar hydrogens and Kollman charges were added to the refined protein structure. The grid maps generated around the receptor was set to 194.185, 174.869, 149.116 as grid centers and grid box sizes of 57, 53, 54 Å and number of points 52, 51, 50 each for X, Y, and Z-axes respectively to represent the 3D space of the binding site. The docking simulations performed with AutoDock Vina and the binding affinity of the ligand observed as a negative score with the unit of kcal/mol. The protein-ligand interactions were visualized and analysed using Biovia Discovery Studio 2019 Client visualizer and the PyMOL Molecular Graphics System, Version 2.0 Schrodinger, [32,33]. The docking results were analyzed to identify the most probable binding mode of the ligand, and the binding energy was calculated to estimate the strength of the interactions [34].

3. Results and discussions

3.1. Spectroscopic study

The structure of the compound **TCA3** was identified and characterized by their spectroscopic data (FT-IR, ^{1H}NMR , and $^{13\text{C}}\text{NMR}$). The obtained IR spectrum of **TCA3** shows bands in the region 3000– 2838 cm $^{-1}$ attributed to the stretching vibrations of C-H aliphatic. In addition, all bands occurred in the region 1400–1230 cm $^{-1}$ are assigned to the deformation vibrations of (C-H). The stretching vibrations of the aromatic C=C groups are located at 1361 cm $^{-1}$. The vibrations of the C=N and aromatic C=C groups are obtained within the range of 1600–2000 cm $^{-1}$.

The structure TCA3 was confirmed by analysis of NMR data. ^{1H}NMR and ^{13C}NMR spectral data of the synthesized compound are also in accordance with the proposed structure and expected numbers of protons and carbon were observed.

3.2. X-ray crystallography

The structure of the compound **TCA3** is determined by the single crystal X-ray diffraction study. The compound **TCA3** crystallizes in the monoclinic crystal system with the space group $P2_1/c$. The asymmetric unit of the compound **TCA3** contains one unique molecule with Z=4. Fig. 1 indicates the *ORTEP* of the compound **TCA3**. The geometrical parameters like

The molecular structure consists of three rings bromophenyl (C1-C2-C3-C4-C5-C6-Br1) ring, thiadiazole ring (S1-C9-N1-N2-C10) and triazine ring (N2-C10-N3-N4-C12-C11), and 3-tertiary butyl group is attached to the triazine ring. The bromophenyl ring and thiadiazole ring are bridged by the ethenyl group and makes a dihedral angle of -177.26° which clearly indicates coplanarity. The crystal structure of the compound TCA3 is stabilized by diverse intermolecular hydrogen bonding interactions and $\pi...\pi$ interactions. The C—H...Br, C—H...O, and C—H...N intermolecular interactions are leading to the formation of the several ring motifs, thereby involved in the stabilization of the compound TCA3, as shown in Fig. 2. Interestingly, intermolecular halogen-based interaction (C15-H15B...Br1), was observed with the distance of 3.048 Å (H15--Br1). The geometry details of these hydrogen bond interactions are given in Table 2.

Apart from hydrogen bond interactions, $\pi...\pi$ interactions are also involved in the compound. The $\pi...\pi$ interactions are existed between the centroid of the thiadiazole ring to the centroid of the 1,2,4-triazine ring of the molecule. Also, one more interaction exists between centroid of the thiadiazole ring to the centroid of the bromophenyl rings of the molecule. The geometry details of these interactions are listed in the Table 3.

3.3. Hirshfeld surface analysis

To identify and understand the key intermolecular interactions exhibited by the structure and its relative contribution to the crystal packing, a detailed Hirshfeld surface analysis was performed [35]. The 2D fingerprint plots (FPs) analysis revealed the contributions of the

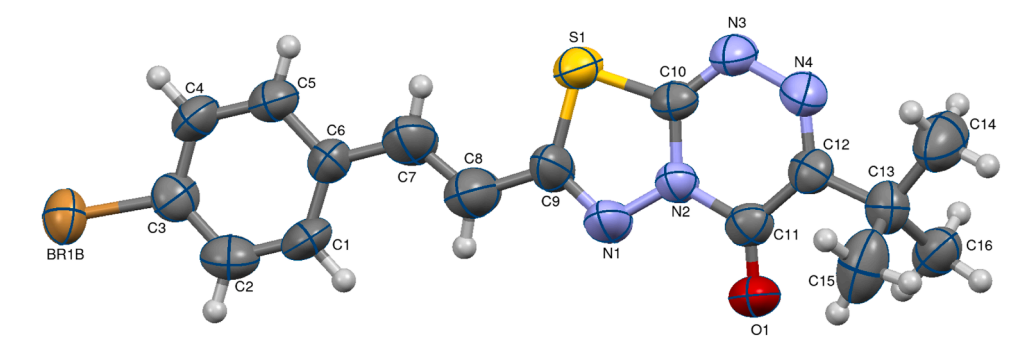


Fig. 1. ORTEP of the compound TCA3.

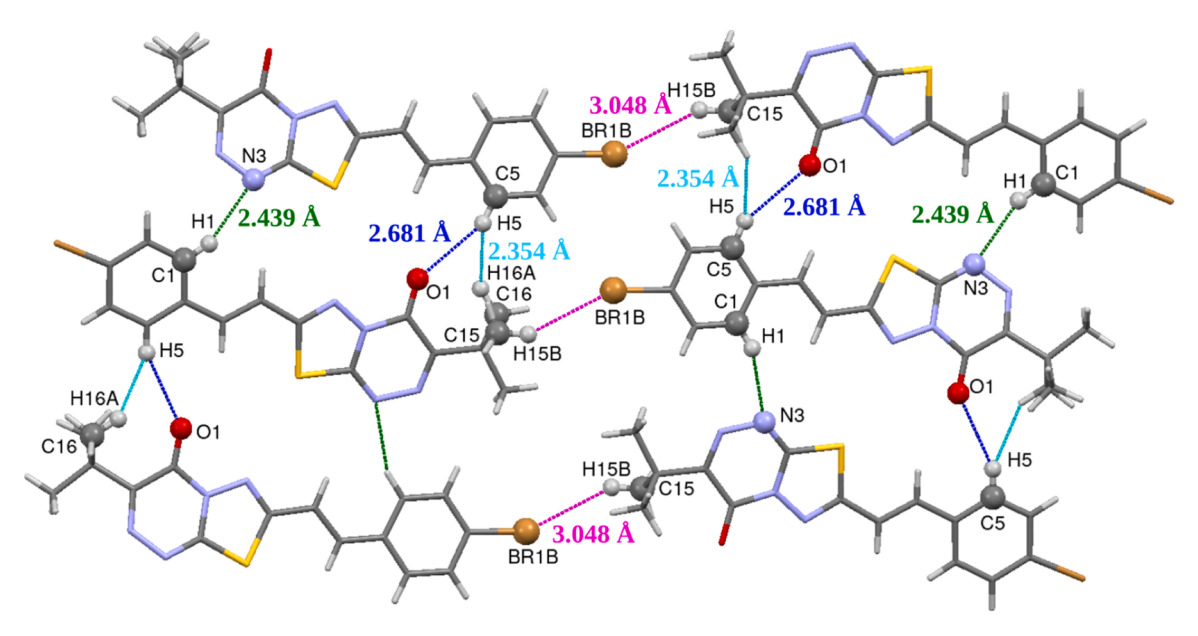


Fig. 2. Various intermolecular interactions such as C—H...Br (Magenta), C—H...O (Blue), C—H...N (Green), C—H...H—C (Cyan) involved in the stabilization of the compound.

Table 2
Geometry details of hydrogen bond interactions involved in the compound TCA3.

D-HA	D-H (Å)	HA (Å)	DA (Å)	D-HA (°)
C1-H1N3	0.93	2.44	3.315(10)	157
C7-H7S1 ^a	0.93	2.70	3.140(9)	110
C15-H15CO1 ^a	0.96	2.53	3.112(15)	119
C16-H16AO1 ^a	0.96	2.46	3.121(9)	126

Symmetry code: i:2-x,1/2 + y,3/2-z a-intramolecular interactions.

interactions between the different atomic pairs [36]. A detailed HS analysis has been carried out to identify the key intermolecular interactions present in the crystal structures and their relative contributions to the crystal packing stability. The contributions from interactions between different atomic pairs were studied with the help of the 2D fingerprint plots (FPs). The Hirshfeld surface of the crystal is mapped over a range of 0.2558 a.u. to 1.5142 a.u. with a transparent surface to

visualize the interactions of the different moieties contributing to the stability of the crystal structure. It was found to exhibit the globularity and asphericity value of 0.717 and 0.534 respectively. The $d_{\rm norm}$ mapped Hirshfeld surface is shown in the Fig. 3. The large circular depressions (red) indicate the strong C—H…N interactions.

The 2D fingerprint plot of the atomic pairs are found to be symmetric, indicating the strong interactions (Fig. 4). The 2D fingerprint plots of the various atomic pairs indicated that the majority of the contribution to the crystal packing is given by the H...H interactions contribute about $33.4\,\%$ to the overall stability of the structure. Further, the other atomic pair interactions such as Br...H, N...H, C...H, O...H and S...H contributes about $14\,\%$, $12.3\,\%$, $12\,\%$, $7.7\,\%$ and $3.8\,\%$ respectively.

The bow tie fashioned (red and blue) triangles observed in the shape index plot and the flat regions observed in the curvedness plot substantiates the presence of the $\pi...\pi$ interactions present in the structure [37]. The shape index and curvedness plot of the structure is shown in the Fig. 5 respectively.

Table 3 Details of π ... π interaction exhibit between centroid of rings.

CgI	CgJ	CgI-CgJ	α (°)	β (°)	γ (°)	$CgI_{\perp}(\mathring{A})$	CgJ_{\perp} (Å)	Slippage (Å)
Cg1	Cg2 ⁱ	3.754(4)	4.4(3)	25.2	24.2	3.424(3)	3.397(3)	1.599
Cg1	Cg3 ⁱⁱ	3.828(4)	2.4(3)	21.8	20.2	-3.593(3)	-3.556(4)	1.419

i: 2-X,1-Y,1-Z; ii: 2-X,1-Y, 2-Z.

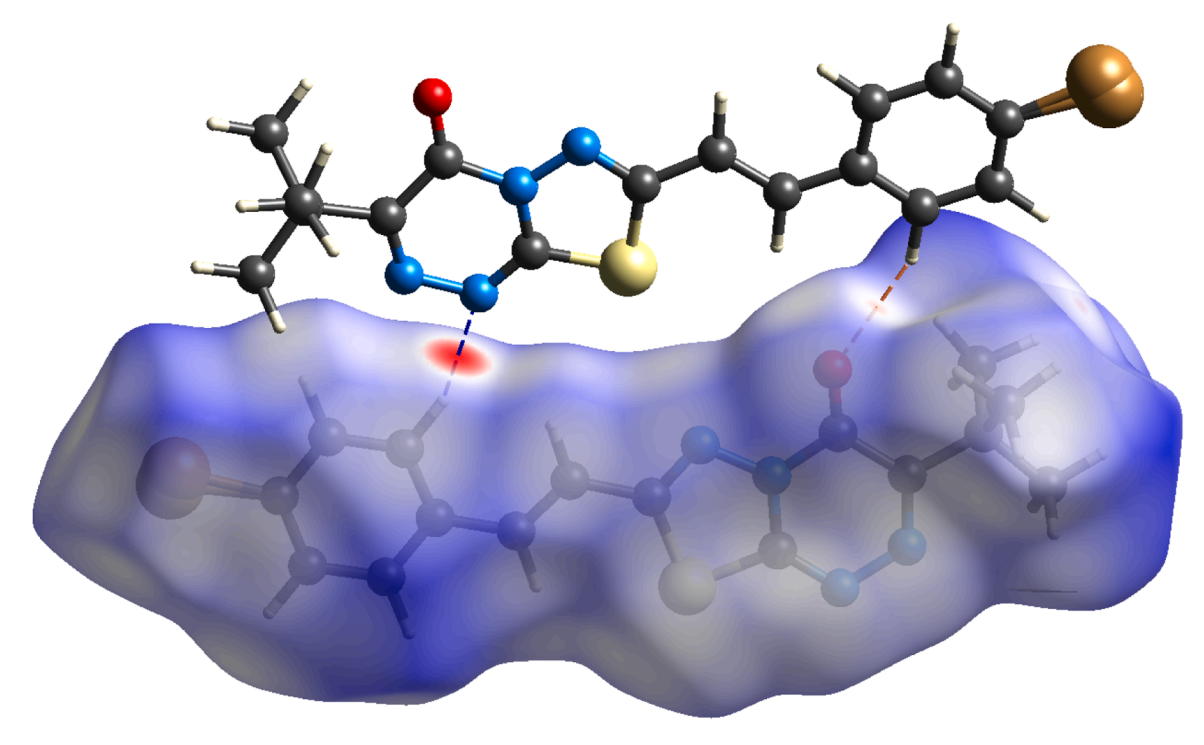


Fig. 3. The d_{norm} mapped Hirshfeld surface revealing the strong C—H...N interactions.

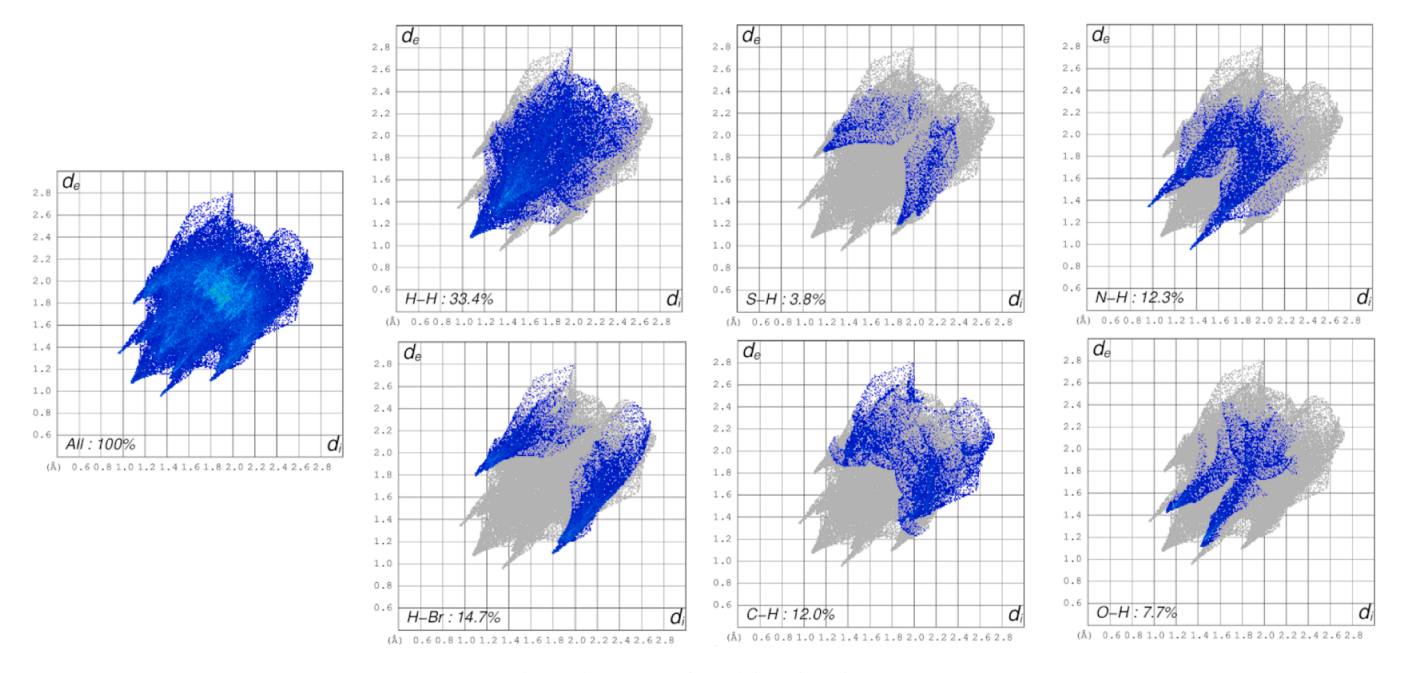


Fig. 4. The 2D fingerprint plots of the selected atomic pairs.

3.4. Interaction energies and 3D energy framework

In order to visualize the supramolecular architecture of the molecules in a crystal and to determine the interaction energies between the molecular pairs in a crystal structure, energy framework and interaction energies analysis have been performed [38]. The energy frameworks were generated for molecules with 3.8 Å radius from the selected molecule using the software CrystalExplorer 17.5 [24]. Fig. 6 shows the energy frameworks generated using different interaction energies like Coulomb (red), dispersion (green) and total energy (blue) along c-axis. The cut off energy was chosen is 5 kJ/mol.

The total interaction energy $(-202.561~kJ~mol^{-1})$ comprises four components electrostatic $(-63.789~kJ~mol^{-1})$, polarization $(-33.005~kJ~mol^{-1})$, dispersion $(-266.425~kJ~mol^{-1})$, and repulsion energy $(160.659~kJ~mol^{-1})$. The individual components of energy and total energy for the specific molecular pairs are listed in Table 4. The values in the Table 4, clearly indicates that the dispersion energy is more dominant energy compare to all other energies.

3.5. Other molecular properties using DFT calculations

Quantum chemistry computations were used to optimize the

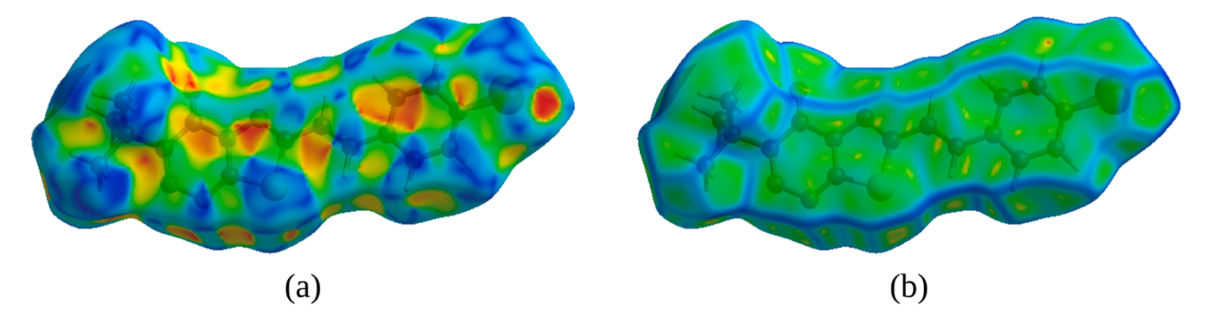


Fig. 5. The shape index plot with the adjacent blue and red triangles indicating the $\pi...\pi$ interactions.

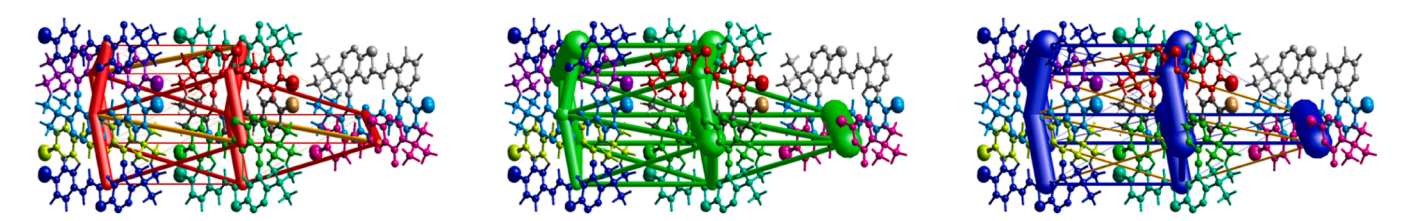


Fig. 6. Graphical representation of the interaction energies Coulomb energy (red), Dispersion energy (green) and Total energy (blue) along a,b, c-axis.

Table 4Different interaction energies of the molecular pairs in kJ/mol.

N	Symmetry operations	R in Å	$E_{ m ele}$	$E_{ m pol}$	$E_{ m dis}$	$E_{ m rep}$	$E_{ m tot}$
1	x, -y+1/2, z+1/2	6.61	5.3	-5.1	-38.1	14.8	-20.2
1	-x, -y, -z	10.67	-2.4	-3.2	-58.1	32.3	-30.6
1	-x, -y, -z	22.72	0.5	-0.1	-3.8	1.0	-2.2
1	-x, -y, -z	4.14	-28.3	-16.0	-98.5	44.7	-91.7
1	-x, y+1/2, -z+1/2	7.92	-37.0	-15.8	-41.6	30.5	-60.7
1	x, y, z	14.05	-3.5	-1.7	-17.3	13.0	-9.7
1	-x, $y+1/2$, $-z+1/2$	19.68	0.8	-0.2	-1.8	0.0	-0.9
1	x, -y+1/2, z+1/2	17.85	-12.4	-1.7	-16.8	44.2	6.9
1	-x, -y, -z	12.83	14.4	-6.9	-19.7	17.6	6.7

The scale factors used for the construction of energy frameworks are $k_e = 1.019$, $k_p = 0.651$, $k_p = 0.901$, $k_p = 0.90$

molecule structures and assess their physical and chemical properties. The *Gaussian 09* program was used to do calculations on the MOL file created by the CIF. Structures were optimized in the gas phase using ω B97X functional with the 6–311+G(d,p) basis set. The absence of imaginary frequencies confirmed that the optimized structure attains minimum energy [39]. The optimized geometrical parameters (Table 5 and 6 respectively) like bond lengths and bond angles are in good correlation with experimental data (crystal structure) obtained from the X-ray diffraction study [39,40]. The superimposition of the experimental and theoretical structure is as shown in Fig. 7, and yields rms deviation of 0.375 Å for the compound TCA3.

The FMOs theory, which involves HOMO and LUMO, is an effective explanation for a molecule's chemical stability. The HOMO and LUMO energies of ligands and complexes indicate energy distribution and energetic behavior. The negative magnitude of E_{HOMO} and E_{LUMO} determines the stability of compounds [41] A molecule's energy gap (E_{HOMO} - E_{LUMO}) determines its chemical reactivity and kinetic stability [42]. A molecule with a wide HOMO-LUMO gap is considered hard, tiny, and less polarizable. Soft systems feature a tiny HOMO-LUMO gap, big

Bond lengths of non-hydrogen atoms of the compound TCA3.

U	, ,				
Atoms	Length (Å)		Atoms	Length (Å)	
	XRD	DFT		XRD	DFT
Br1A-C3	1.86(1)	1.895	C1-C6	1.36(1)	1.399
S1-C9	1.734(7)	1.767	C2-C3	1.36(1)	1.391
S1-C10	1.718(8)	1.750	C3-C4	1.36(1)	1.388
N1-N2	1.365(8)	1.364	C4-C5	1.38(1)	1.387
O1-C11	1.212(9)	1.204	C5-C6	1.38(1)	1.397
N1-C9	1.29(1)	1.288	C6-C7	1.43(1)	1.465
N2-C10	1.353(9)	1.370	C7-C8	1.35(1)	1.337
N2-C11	1.410(9)	1.409	C8-C9	1.45(1)	1.451
N3-N4	1.380(9)	1.367	C11-C12	1.46(1)	1.485
N3-C10	1.281(9)	1.285	C12-C13	1.51(1)	1.526
N4-C12	1.288(9)	1.297	C13-C14	1.53(1)	1.532
C1-C2	1.35(1)	1.384	C13-C15	1.54(1)	1.541
C13-C16	1.53(1)	1.541			

Table 6
Bond angles of non-hydrogen atoms of the compound TCA3.

Atoms	Angle (°)		Atoms	Angle (°)	le (°)	
	XRD	DFT		XRD	DFT	
C9-S1-C10	87.6(3)	87.84	S1-C9-N1	117.4(6)	115.70	
N2-N1-C9	107.7(6)	110.30	S1-C9-C8	123.0(6)	123.55	
N1-N2-C10	117.8(6)	117.33	N1-C9-C8	119.4(7)	120.75	
N1-N2-C11	121.4(6)	121.62	S1-C10-N2	109.4(5)	108.83	
C10-N2-C11	120.7(6)	121.05	S1-C10-N3	124.9(5)	125.35	
N4-N3-C10	115.9(6)	116.57	N2-C10-N3	125.7(7)	125.82	
N3-N4-C12	122.6(6)	122.74	O1-C11-N2	120.7(7)	121.61	
C2-C1-C6	121.1(8)	121.00	O1-C11-C12	128.4(7)	127.94	
C1-C2-C3	120.2(8)	119.43	N2-C11-C12	111.0(6)	110.45	
Br1A-C3-C2	115.1(8)	119.51	N4-C12-C11	123.0(6)	123.38	
Br1A-C3-C4	124.6(8)	119.64	N4-C12-C13	117.8(6)	118.14	
C2-C3-C4	120.3(7)	120.85	C11-C12-C13	119.2(6)	118.48	
C3-C4-C5	119.0(7)	119.08	C12-C13-C14	110.8(6)	110.38	
C4-C5-C6	120.9(7)	121.34	C12-C13-C15	108.2(6)	109.50	
C1-C6-C5	118.4(7)	118.29	C12-C13-C16	111.7(7)	109.09	
C1-C6-C7	121.7(8)	122.78	C14-C13-C15	108.5(7)	108.83	
C5-C6-C7	119.9(7)	118.94	C14-C13-C16	107.7(6)	108.94	
C6-C7-C8	125.7(9)	126.16	C15-C13-C16	109.9(7)	110.08	
C7-C8-C9	122.3(8)	124.45				

size, and strong polarizability. A big HOMO-LUMO gap indicates strong molecular stability and aromaticity, but low reactivity in chemical processes [43–45]. A narrow HOMO-LUMO gap indicates anti-aromaticity. HOMO and LUMO energies indicate the ability to donate and acquire electrons, respectively. Molecules with high HOMO energy are more reactive when reacting with electrophiles, while those with low LUMO energy react with nucleophiles. The Fig. 8 indicates the HOMO-LUMO orbitals of the molecule TCA3.

As can be seen from the Fig. 8, the HOMO is completely localized over entire molecule whereas LUMO is localized on 1,3,4-thiadiazolo moiety. The energy gap of the molecule is found to be 4.592 eV. A various reactivity descriptors can be determined using the HOMO and LUMO energies. The larger HOMO - LUMO energy gap indicates the harder and more stable/less reactive molecule [46]. The ionization potential (I) (6.958 eV) describes an atom's ability to give electrons. The energy of the HOMO represents ionization energy. Electron affinity (A) (2.366 eV) describes a ligand's ability to take an electron from the donor. The energy of the LUMO indicates the electron affinity. Electronegativity (χ) describes an atom's ability to attract a pair of electrons. The chemical potential (μ) (-4.662 eV) represents the change in free energy of the system when a particle is added or removed. Chemical hardness (n) indicates a molecule's better kinetic stability and lower reactivity. In terms of energy gap, the larger the gap, the greater the chemical hardness. The chemical hardness is 3.81 eV, which is modest; thus, the compound is chemically stable. Chemical softness (σ) (0.436 eV^{-1}) is the opposite of chemical hardness. Electrophilicity (ω) is the amount of energy lowered when electrons move from donor to acceptor. This energy is assessed using an electrophilicity index. The TCA3 molecule possesses an electrophilicity index of 4.733 eV in the gas phase, ensuring substantial energy transition between HOMO and

LUMO. The molecule with a higher or lower electrophilicity index is known as an electrophile or nucleophile, respectively.

The molecular electrostatic potential (MEP) map is displayed in the Fig. 9. It is useful to study the reactive sites present in the molecule [47]. The importance of MEP lies in the fact that it simultaneously displays molecular size, shape as well as positive, negative and neutral electrostatic potential regions in terms of colour grading (Fig. 9) and is very useful in research of molecular structure with its physiochemical property relationship. The resulting surface simultaneously displays molecular size and shape and electrostatic potential value. The various electrostatic potential values are represented by different colors.

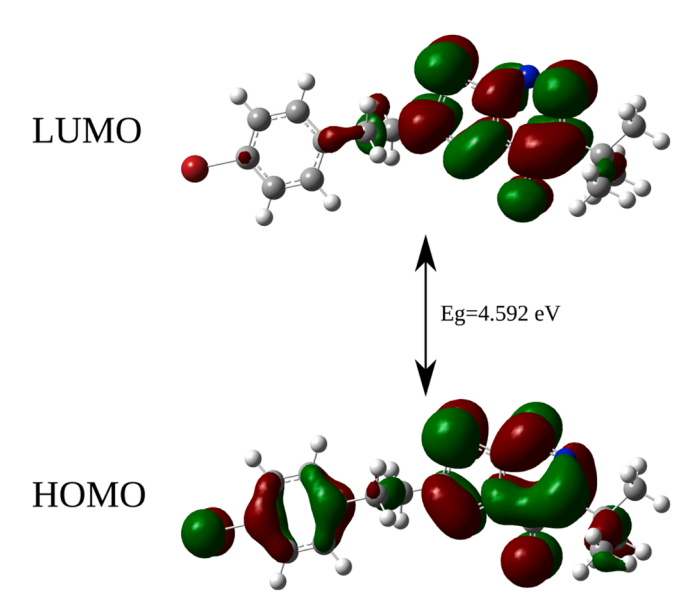


Fig. 8. HOMO-LUMO of the compound TCA3.

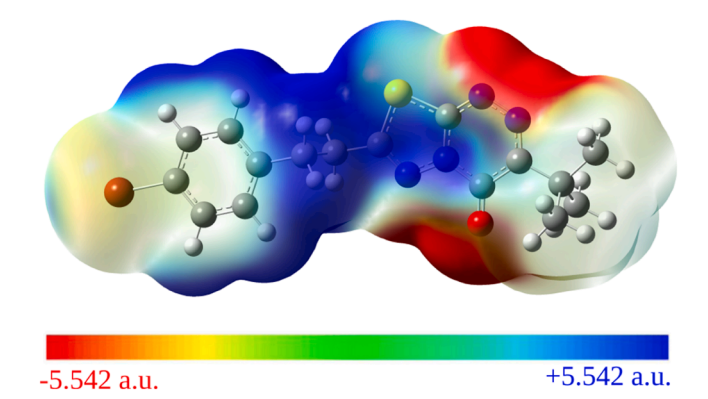


Fig. 9. MEP map of the compound TCA3.

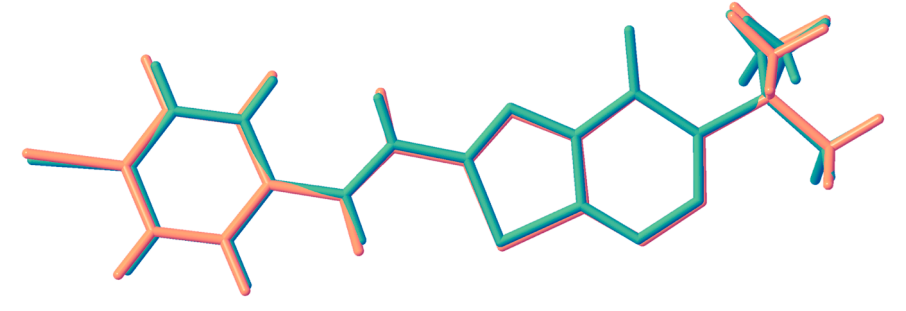


Fig. 7. Superimposition of the two structures obtained from XRD (pink) and DFT (teal) of the compound TCA3.

Potential increasing sequences: red < orange < yellow < green < blue. As cen bee seen from the Fig. 9, the electrophilic region (red color) appear around the nitrogen atoms of the thiadizolo ring and Oxygen atom of the carbonyl group whereas nucleophilic region (blue color) regions appear around the hydrogen atoms of the molecule, mainly around the -CH $_2$ groups of the molecule.

The reduced density gradient (RDG) is used to evaluate the molecular bonding and nonbonding interaction regions in the non-covalent interactions (NCI) approach, which was proposed by Johnson et al. [48]. Through color codes, the isosurfaces directly depict the many types of NCI in real space. It makes it possible to determine the interactions' relative strength on a qualitative yet visual basis, as well as their attractive or repulsive qualities. severe attraction (H-bonding), extremely weak interaction (van der Waals attraction), and severe repulsion (steric repulsion) are indicated by the colors blue, green, and red, respectively.

The green colored isosurfaces in the Fig. 10 clearly indicates the existence of C—H…O and C—H…N interactions. The red Coloured spike in the aromatic rings indicates the existence of steric repulsion between the atoms of the aromatic rings.

3.6. In-silico analysis

3.6.1. ADME-T analysis

The exploration of the physicochemical and ADMET properties of the compound using computational techniques will helps to save lot of resources and it is much more economical as it will prevent the failure of the compound to be drug in the later state or in showing side effects once it has been approved as drug [49].

Several physicochemical properties such as, molecular weight (MW), hydrogen bond donors (HBD), hydrogen bond acceptors (HBA), number of rotatable bonds (RB) and partition co-efficient (Log P) for the TCA3 molecule is analysed and it is observed that all the properties lie in the satisfactory range [50]. In addition, follow Lipinski's rule of five (Ro5), Jorgensen's Ro3, Ghose filter, Vebers's, Egan's, and Muegge's rules for oral bioavailable drugs [51]. Lipinski's rule of 5 (Ro5) suggested that molecules whose properties fell outside the stated boundaries would be less likely to be orally absorbed. While Ro5 does provide some heuristic guidance, there are many factors, which can be used as part of a drug discovery optimization process. In the discovery setting 'the rule of 5' predicts that the approaches in estimate solubility and permeability, poor absorption or permeation is more likely when there are more than 5 H-bond donors. 10 H-bond acceptors, the molecular weight (MWT) is greater than 500 and the calculated Log P (CLogP) is greater than 5 (or MlogP > 4.15) [52].

Compared drug-likeness predictions with their bioavailability scores and toxicity profiles are provided in Table 7 and 8. The SwissADME

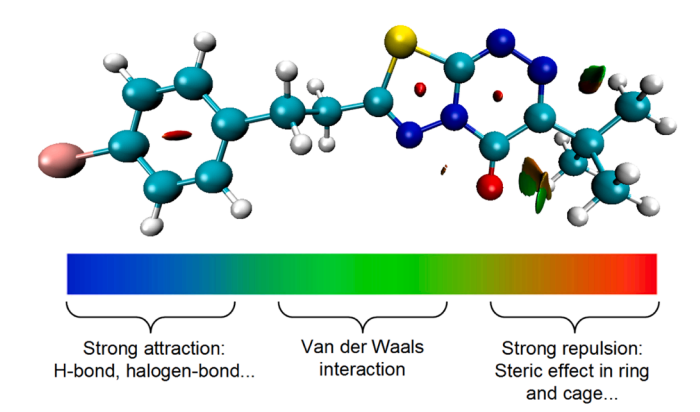


Fig. 10. Non-covalent interactions (NCI) isosurfaces of electron density for the compound **TCA3**. BGR (blue-green-red) color scheme used for plotting isosurfaces of electron density.

analysis revealed that the synthesized compound physiocochemical properties were found to be optimal range and the boiled egg model revealed that the compound possess good gastrointestinal abosorption property of about 95.48 % (Fig. 11(a)). The six descriptors such as LIPO, lipophilicity; SIZE, molecular weight; POLAR, polarity; INSOLU, insolubility; INSATU, unsaturation; FLEX, flexibility, show us that the compound exist within the pink region of radar are considered to possess good bioavailability property in the body. In general, the compound under investigation is showing excellent bioavailability radar properties (Fig. 11(b)).

The other ADMET parameters were evaluated and the water solubility, Caco2 permeability and skin permeability of the compound was found to be -4.592 (log mol/L), 1.502 (log P_{app} in 10^{-6} cm/s) and -5.252 (log K_p) respectively. The ccompound is found be P-glycoprotein I and II inhibitor. The blood brain barrier and central nervous system permeability was found to be 0.475 and -1.943 respectively. The compound showed inhibition activity against CYP3A4, CYP1A2 and CYP2C19. The total clearance value of the compound is found to be less (-0.162) (log ml/min/kg). Further, the compound showed no AMES toxicity with oral rat acute toxicity and oral rat chronic toxicity of 2.264 and 1.512 respectively. All these parameters are tabulated in the Table 7.

3.6.2. Molecular docking analysis

The molecular docking analysis revealed that the binding score of the compound is found to be -8.2 kcal/mol and the corresponding pose with the interactions is shown in the Fig. 12. Further, the binding score of the compound is compared with that of the standard drug Remdesivir which showed the binding score to be -8.6 kcal/mol.

Interestingly, three conventional hydrogen bonding interactions are observed between the oxygen atoms of the amino acid residues THR376, SER496, TYR501 with the nitrogen and sulfur atom of the 1,3,4-thidiazole ring and nitrogen atom of the triazin ring with the distance of 3.28 Å, 3.65 Å and 3.16 Å respectively. The oxygen atom of amino acid TYR501 is bridged with the sulfur atom of the 1,3,4-thidiazole ring through sulfer-X bonding interaction with the distance of 3.19 Å. The π -cation interaction is observed between the centroid of the triazin ring and the nitrogen atom of the ARG498 amino acid at the distance of 3.61 Å. The π -donor interaction is observed between the centroid of the bromophenethyl ring and nitrogen atom of the amino acid PHE377 with the distance of 3.50 Å, where the nitrogen atom of the amino acid residue PHE377 acts as the donor atom in the interaction. The π -alkyl interactions were observed between carbon atom of the amino acids LYS378 and ARG408 with the centroids of the triazin ring and the centroid of the bromophenethyl ring respectively, along with this alkyl interactions were also found between the carbon atoms of the amino acids ARG493 and LEU455 with the bromine atom of the bromophenethyl ring of the molecule. The 2D interaction of the ligand with the protein is shown in the Fig. 12(b).

Further, the superposition of the synthesized ligand and the Remdesivir showed that both the compounds occupies the same region in the protein (Fig. 13 and 14). The amino acids interaction with the synthesized ligand and the Remdesivir ligand are given in the Table 9.

4. Conclusion

In summary, the novel thiadiazole-triazine compound TCA3 is synthesized and characterized by NMR and X-ray diffraction study to explore various properties of the compound. The crystal structure is

Table 7Comparison of the physicochemical properties of the compound.

Compound	Molecular weight	HBA	Rotatable bonds	Surface area Å ²	Log P
TCA3	391.29	6	2	145.382	3.6023

Table 8ADMET profiles of the synthesized compound.

ADMET prope	erties	Compound TCA3	
Absorption	Water solubility	-4.592 log mol/L	
	Caco2 permeability	1.502 log Papp in 10 ⁻⁶ cm/s	
	Intestinal absorption (human)	95.486%	
	Skin permeability	-5.252 log Kp	
	P-glycoprotein substrate	No	
	P-glycoprotein I inhibitor	Yes	
	P-glycoprotein II inhibitor	Yes	
Distribution	VDss (human)	−0.267 log L/kg	
	Fraction unbound (human)	0.052 Fu	
	BBB permability	0.475 log BB	
	CNS permability	-1.943 log PS	
Metabolism	CYP2D6 substrate	No	
	CYP3A4 substrate	Yes	
	CYP1A2 inhibitor	Yes	
	CYP2C19 inhibitor	Yes	
	CYP2D6 inhibitor	No	
	CYP3A4 inhibitor	No	
Excretion	Total clearance	-0.162 log ml/min/kg	
	Renal OCT2 substrate	No	
Toxicity	AMES toxicity	No	
	Maximum tolerated dose (human)	0.293 log mg/kg/day	
	hERG I inhibitor	No	
	hERG II inibitor	No	
	Oral Rat Acute Toxicity (LD50)	2.264 mol/kg	
	Oral Rat Chronic Toxicity (LOAEL)	1.512 log mg/kg_bw/day	
	Hepatotxicity	Yes	
	Skin Sensitization	No	

stabilized by the various intermolecular and intramolecular interactions. The Hirshfeld surface and fingerprint analyses revealed that the H...H contacts are the major contributors to the total Hirshfeld surface of about 33.4 %. Interaction energy and energy framework analysis indicates that dispersion energy is more dominant over the other energies in the synthesized compound. The HOMO-LUMO energy gap of the molecule is found to be 4.592 eV. Further, MEP surface plot revealed that the compound showed good hydrogen bond interaction regions helpful for the interactions with the biological molecules. Further, the ADMET analysis revealed that the compound possess good gastrointestinal absorption property of about 95.48 % and all the six descriptors were found to be within the acceptable limit indicating good bioavailability property. The compound showed the blood brain barrier penetration ability and the value is found to be 0.475 and also the compound showed no AMES toxicity making it suitable for its usage as drug. The molecular docking analysis revealed that the compound showed good inhibition activity against the Omicron protein with the binding score of -8.2 kcal/mol and the binding region of the compound to be the same as that of the Remdesivir a standard drug used extensively for the treatment of COVID. Hence, our research work explores the antiviral property of the synthesized thiadiazole-triazine and its ADMET property revealed that the compound showed good drug property. Further, invitro analysis have to be performed to explore the potential of the compound.

CRediT authorship contribution statement

Lohith T. N.: Writing - review & editing, Supervision. Chandra:

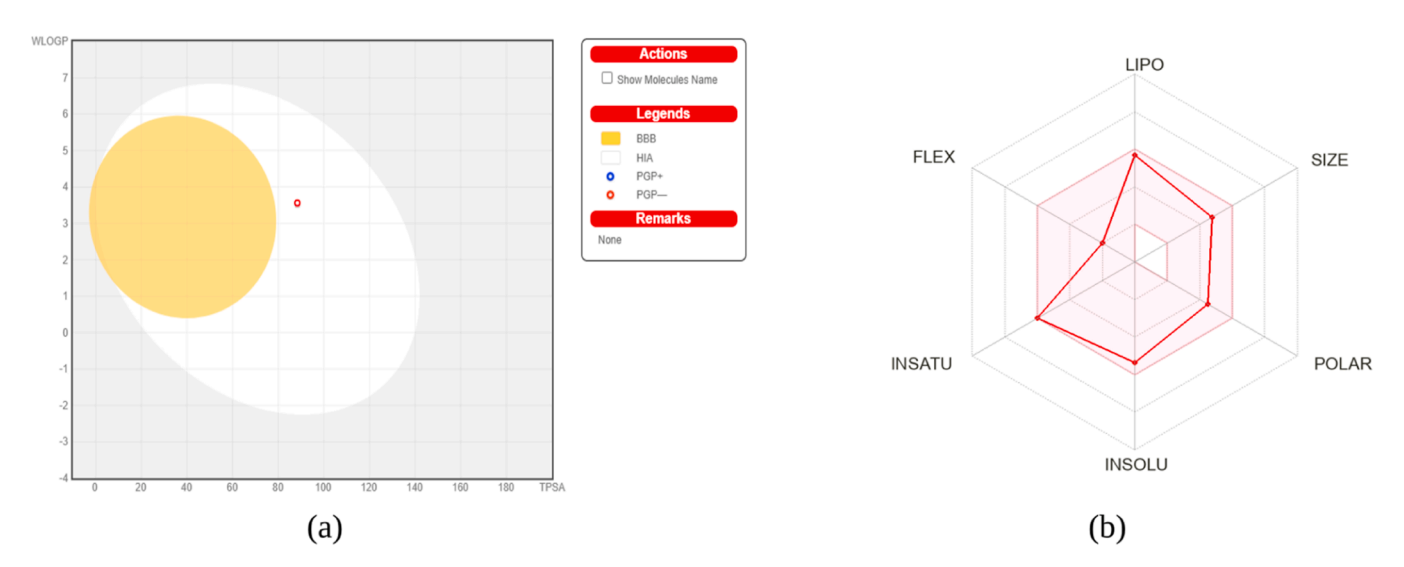


Fig. 11. Bioavailability radar of the compound under study BOILED-Egg model (a) and for prediction of GI absorption and brain penetration (b).

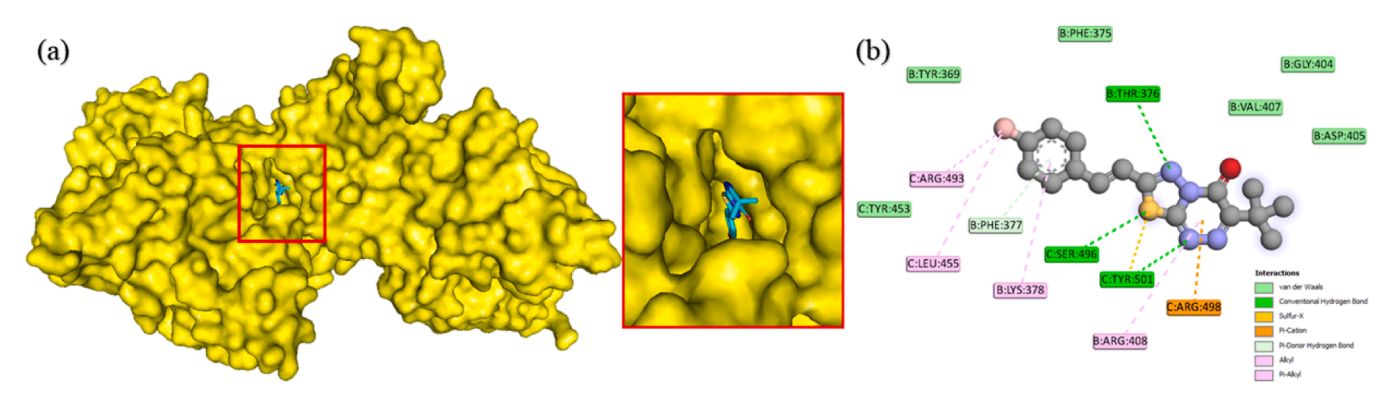


Fig. 12. (a) Binding pose of the ligand with the protein and (b) 2D interaction of the ligand revealing the amino acids with which the ligand is interacting.

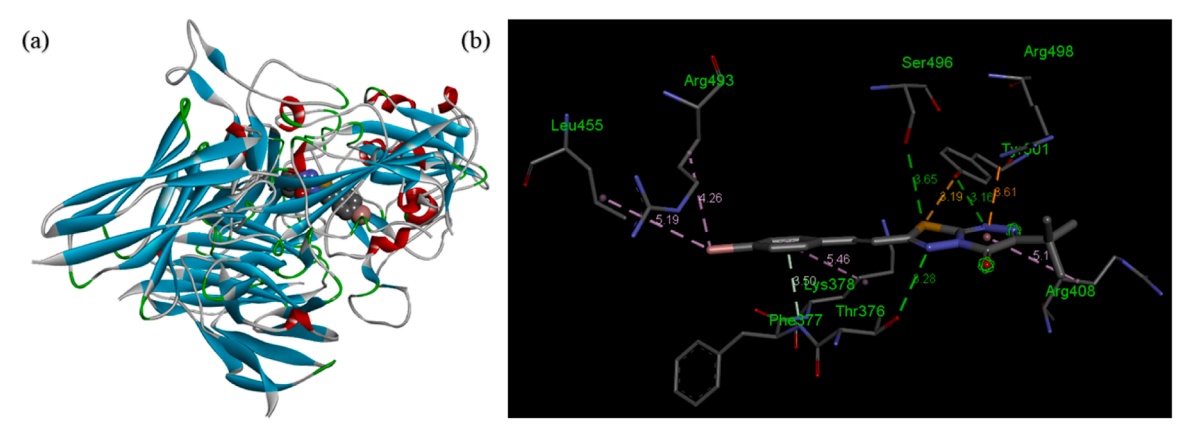


Fig. 13. 2D interaction plot of the protein-ligand complex along with its distances.

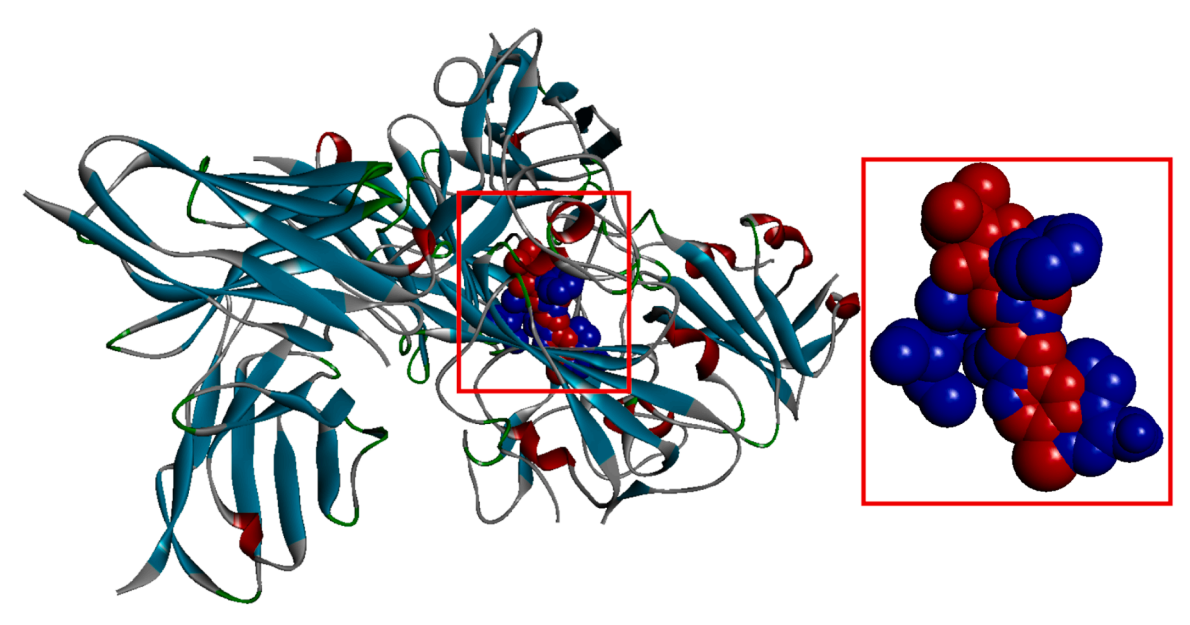


Fig. 14. Cartoon view of the docking of the combined ligand (red colour) and the standard drug remdesivir (dark blue colour) with Omicron variant of SARS-CoV-2 spike protein.

Table 9
The binding affinity of the synthesized compound (TCA3) and Remdesivir with protein and their corresponding; interactions.

Mode	Binding Affinity (kcal/mol)	Amino Acid Residues
TCA3	-8.2	PHEB374, PHEB377, ARGC493, LEUB455, PROB384, ARGC403, LYSB378, PHEB375
Remedesivir	-8.6	ARGC493, LEUC455, ARGC403, LYSB378, ILEI57, TYRC449, THRB376, PHEB377, ARGC498, SERC496, TYRC501, ARGB408, TYRC453, SERC496, TYRC501, ARGB408, VALB407

Writing – original draft, Software, Formal analysis. **Gayathri B. H.:** Methodology, Formal analysis. **Shamantha Kumar:** Visualization, Validation. **Shivaprasad C. M.:** Formal analysis, Data curation. **Divya K.:** Validation, Conceptualization. **Sridhar M. A.:** Writing – review & editing, Supervision. **Mahendra M.:** Investigation, Formal analysis.

Declaration of competing interest

The authors declare that they have no known competing financial

interests or personal relationships that could have appeared to influence the work reported in this paper.

Data availability

Data will be made available on request.

Supplementary materials

Supplementary material associated with this article can be found, in the online version, at doi:10.1016/j.molstruc.2024.139133.

References

- R.M. Abdel-Rahman, M.A. Ibrahim, T.E.S. Ali, 1, 2, 4-Triazine Chemistry Part II: Synthetic approaches for phosphorus containing 1, 2, 4-triazine derivatives, European Journal of Chemistry 1 (2010) 388–396.
- [2] K. Sztanke, K. Pasternak, M. Sztanke, M. Kandefer-Szerszeń, A.E. Koziol, I. Dybała, Crystal structure, antitumour and antimetastatic activities of disubstituted fused 1, 2, 4-triazinones, Bioorg. Med. Chem. Lett. 19 (2009) 5095–5100.
- [3] R. Mohebat, M. Tabatabaee, M.A. Bafghi, An efficient synthesis of [1, 3, 4] thiadiazolo [2, 3-c][1, 2, 4] triazin-4-ones, Journal of Sulfur Chemistry 34 (2013) 377–382.

- [4] K.M. Chandini, T.N. Lohith, S. Shamanth, M.A. Sridhar, K. Mantelingu, N. K. Lokanath, Synthesis, structure elucidation, energy frameworks, and DFT calculations of 2,5-diphenyl-1,3,4-thiadiazole, J. Mol. Struct. 1283 (2023) 135320, https://doi.org/10.1016/j.molstruc.2023.135320.
- [5] R.R. Bartlett, U. Gebert, B. Kerekjarto, R. Schleyerbach, W. Thorwart, K. U. Weithmann, Substituted 3-phenyl-7H-thiazolo (3, 2-b)(1, 2, 4) triazin-7-ones as antiinflammatory agents with immunomodulating properties, Drugs Exp. Clin. Res. 15 (1989) 521–526.
- [6] H. Tahtaci, H. Karacık, A. Ece, M. Er, M.G. Şeker, Design, synthesis, SAR and molecular modeling studies of novel imidazo [2, 1-b][1, 3, 4] thiadiazole derivatives as highly potent antimicrobial agents, Mol. Inform. 37 (2018) 1700083.
- [7] M. Er, B. Ergüven, H. Tahtaci, A. Onaran, T. Karakurt, A. Ece, Synthesis, characterization, preliminary SAR and molecular docking study of some novel substituted imidazo [2, 1-b][1, 3, 4] thiadiazole derivatives as antifungal agents, Medicinal Chemistry Research 26 (2017) 615–630.
- [8] N. Houas, S. Kitouni, N. Chafai, S. Ghedjati, M. Djenane, A. Tounsi, New biphosphonate derivative: Synthesis, characterization, antioxidant activity in vitro and via cyclic voltammetry mode and evaluation of its inhibition of SARS-CoV-2 main protease, J. Mol. Struct. 1284 (2023) 135356.
- [9] M. Elkolli, N. Chafai, S. Chafaa, I. Kadi, C. Bensouici, A. Hellal, New phosphinic and phosphonic acids: Synthesis, antidiabetic, anti-Alzheimer, antioxidant activity, DFT study and SARS-CoV-2 inhibition, J. Mol. Struct. 1268 (2022) 133701.
- [10] N. Chafai, O. Moumeni, S. Chafaa, Novel α-aminophosphonate derivates synthesis, theoretical calculation, Molecular docking, and in silico prediction of potential inhibition of SARS-CoV-2, J. Mol. Struct. 1272 (2023) 134196.
- [11] A. Tabbiche, A. Bouchama, N. Chafai, F. Zaidi, C. Chiter, M. Yahiaoui, A. Abiza, New bis hydrazone: synthesis, X-ray crystal structure, DFT computations, conformational study and in silico study of the inhibition activity of SARS-CoV-2, J. Mol. Struct. 1261 (2022) 132865.
- [12] L. Adjissi, N. Chafai, K. Benbouguerra, I. Kirouani, A. Hellal, H. Layaida, M. Elkolli, C. Bensouici, S. Chafaa, Synthesis, characterization, DFT, antioxidant, antibacterial, pharmacokinetics and inhibition of SARS-CoV-2 main protease of some heterocyclic hydrazones, J. Mol. Struct. 1270 (2022) 134005.
- [13] H. Tlidjane, N. Chafai, S. Chafaa, C. Bensouici, K. Benbouguerra, New thiophene-derived α-aminophosphonic acids: Synthesis under microwave irradiations, antioxidant and antifungal activities, DFT investigations and SARS-CoV-2 main protease inhibition, J. Mol. Struct. 1250 (2022) 131853.
- [14] K. Benbouguerra, N. Chafai, S. Chafaa, Y.I. Touahria, H. Tlidjane, New α-Hydrazinophosphonic acid: synthesis, characterization, DFT study and in silico prediction of its potential inhibition of SARS-CoV-2 main protease, J. Mol. Struct. 1239 (2021) 130480.
- [15] M. Kurbanova, M. Ashfaq, A. Sadigova, M. Feizi-Dehnayebi, A. Maharramov, M. N. Tahir, A Hydrazone Derivative: Synthesis, Crystal Structure, Supramolecular Assembly Exploration by Hirshfeld Surface Analysis and Computational Study, Journal of Structural Chemistry 65 (2024) 92–106.
 [16] M. Milusheva, M. Todorova, V. Gledacheva, I. Stefanova, M. Feizi-Dehnayebi,
- [16] M. Milusheva, M. Todorova, V. Gledacheva, I. Stefanova, M. Feizi-Dehnayebi, M. Pencheva, P. Nedialkov, Y. Tumbarski, V. Yanakieva, S. Tsoneva, Novel anthranilic acid hybrids—An alternative weapon against inflammatory diseases, Pharmaceuticals 16 (2023) 1660.
- [17] Z. Akbari, C. Stagno, N. Iraci, T. Efferth, E.A. Omer, A. Piperno, M. Montazerozohori, M. Feizi-Dehnayebi, N. Micale, Biological evaluation, DFT, MEP, HOMO-LUMO analysis and ensemble docking studies of Zn (II) complexes of bidentate and tetradentate Schiff base ligands as antileukemia agents, J. Mol. Struct. 1301 (2024) 137400.
- [18] A.E. Owen, H. Louis, E.C. Agwamba, A.D. Udoikono, A.L.E. Manicum, Antihypotensive potency of p-synephrine: Spectral analysis, molecular properties and molecular docking investigation, J. Mol. Struct. 1273 (2023) 134233.
- [19] R.T. Eastman, J.S. Roth, K.R. Brimacombe, A. Simeonov, M. Shen, S. Patnaik, M. D. Hall, Remdesivir: a review of its discovery and development leading to emergency use authorization for treatment of COVID-19, ACS. Cent. Sci. 6 (2020) 672–683.
- [20] G.M. Sheldrick, SHELXT-Integrated space-group and crystal-structure determination, Acta Crystallographica Section A: Foundations and Advances 71 (2015) 3–8.
- [21] G.M. Sheldrick, Crystal structure refinement with SHELXL, Acta Crystallographica Section C: Structural Chemistry 71 (2015) 3–8.
- [22] A.L. Spek, Structure validation in chemical crystallography, Acta Crystallographica Section D: Biological Crystallography 65 (2009) 148–155.
- [23] C.F. Macrae, I. Sovago, S.J. Cottrell, P.T. Galek, P. McCabe, E. Pidcock, M. Platings, G.P. Shields, J.S. Stevens, M. Towler, Mercury 4.0: From visualization to analysis, design and prediction, J. Appl. Crystallogr. 53 (2020) 226–235.
- [24] P.R. Spackman, M.J. Turner, J.J. McKinnon, S.K. Wolff, D.J. Grimwood, D. Jayatilaka, M.A. Spackman, CrystalExplorer: A program for Hirshfeld surface analysis, visualization and quantitative analysis of molecular crystals, J. Appl. Crystallogr. 54 (2021) 1006–1011.
- [25] M. Frisch, F. Clemente, Gaussian 09, revision a. 01, mj frisch, gw trucks, hb schlegel, ge scuseria, ma robb, jr cheeseman, g, Scalmani, V. Barone, B. Mennucci, GA Petersson, H. Nakatsuji, M. Caricato, X. Li, HP Hratchian, AF Izmaylov, J. Bloino, G. Zhe (2009) 20–44.
- [26] L. Tumakuru Nagarajappa, S. Chikkappaiahnayaka, M. Benedict Leoma, B. K. Isamura, K. Venkatesh, K.R. Singh, K. Sindogi, S. Mandayam Anandalwar, M. P. Sadashiva, Unraveling the crystal structure, stability and drug likeness of 1, 3, 4-oxadiazole derivatives against Myelofibrosis: a combined experimental and computational investigation, Journal of Biomolecular Structure and Dynamics (2024) 1–15.

- [27] T. Lu, F. Chen, Multiwfn: A multifunctional wavefunction analyzer, J. Comput. Chem. 33 (2012) 580–592.
- [28] W. Humphrey, A. Dalke, K. Schulten, VMD: visual molecular dynamics, J. Mol. Graph. 14 (1996) 33–38.
- [29] X. Zhang, F. Luo, H. Zhang, H. Guo, J. Zhou, T. Li, S. Chen, S. Song, M. Shen, Y. Wu, A cocktail containing two synergetic antibodies broadly neutralizes SARS-CoV-2 and its variants including Omicron BA, 1 and BA. 2, bioRxiv. (2022), 2022.04. 26.489529.
- [30] G.M. Morris, R. Huey, W. Lindstrom, M.F. Sanner, R.K. Belew, D.S. Goodsell, A. J. Olson, AutoDock4 and AutoDockTools4: Automated docking with selective receptor flexibility, J. Comput. Chem. 30 (2009) 2785–2791.
- [31] J. Eberhardt, D. Santos-Martins, A.F. Tillack, S. Forli, AutoDock Vina 1.2. 0: New docking methods, expanded force field, and python bindings, J. Chem. Inf. Model. 61 (2021) 3891–3898.
- [32] D.S. Biovia, Discovery studio modeling environment, Release (2017).
- [33] W.L. DeLano, The PyMOL molecular graphics system, http://www.pymol. Org/(2002).
- [34] L. Tumakuru Nagarajappa, K. Ravi Singh, B. Kabuyaya Isamura, K.S. Vinay Kumar, S. Mandayam Anandalwar, M.P. Sadashiva, SARS-CoV-2 Mpro binding profile and drug-likeness of two novel thiazole derivatives: structural elucidation, DFT studies, ADME-T and molecular docking simulations, Journal of Biomolecular Structure and Dynamics 41 (2023) 11122–11136, https://doi.org/10.1080/ 07391102.2022.2159880.
- [35] M.A. Spackman, D. Jayatilaka, Hirshfeld surface analysis, CrystEngComm. 11 (2009) 19–32.
- [36] M.A. Spackman, J.J. McKinnon, Fingerprinting intermolecular interactions in molecular crystals, CrystEngComm. 4 (2002) 378–392.
- [37] J.J. Koenderink, A.J. Van Doorn, Surface shape and curvature scales, Image Vis. Comput. 10 (1992) 557–564.
- [38] C.F. Mackenzie, P.R. Spackman, D. Jayatilaka, M.A. Spackman, CrystalExplorer model energies and energy frameworks: extension to metal coordination compounds, organic salts, solvates and open-shell systems, IUCrJ. 4 (2017) 575–587.
- [39] M. B, Y.D. Bodke, S.K.J. R, L.T. N, S.M. A, Novel Isoxazolone Based Azo Dyes: Synthesis, Characterization, Computational, Solvatochromic UV–Vis Absorption and Biological Studies, J. Mol. Struct. 1244 (2021) 130933, https://doi.org/ 10.1016/i.molstruc.2021.130933.
- [40] M.N. Tahir, K.S. Munawar, M. Feizi-Dehnayebi, M. Ashfaq, M.E. Muhammed, One-dimensional polymer of copper with salicylic acid and pyridine linkers: Synthesis, characterizations, solid state assembly investigation by hirshfeld surface analysis, and computational studies, J. Mol. Struct. 1297 (2024) 136956.
- [41] M. B, Y.D. Bodke, N. O, L.T. N, N. G, S. Ma, Coumarin-Benzothiazole Based Azo Dyes: Synthesis, Characterization, Computational, Photophysical and Biological Studies, J. Mol. Struct. 1246 (2021) 131170, https://doi.org/10.1016/j. molstruc.2021.131170.
- [42] K. Upendranath, T. Venkatesh, T.N. Lohith, M.A. Sridhar, Synthesis, characterizations of new Schiff base heterocyclic derivatives and their optoelectronic, computational studies with level II & III features of LFPs, J. Mol. Struct. 1264 (2022) 133231, https://doi.org/10.1016/j.molstruc.2022.133231.
- [43] H.S.N. Prasad, A.P. Ananda, T.N. Lohith, P. Prabhuprasad, H.S. Jayanth, N. B. Krishnamurthy, M.A. Sridhar, L. Mallesha, P. Mallu, Design, synthesis, molecular docking and DFT computational insight on the structure of Piperazine sulfynol derivatives as a new antibacterial contender against superbugs MRSA, J. Mol. Struct. 1247 (2022) 131333, https://doi.org/10.1016/j.molstruc.2021.131333.
- [44] T.N. Lohith, M.K. Hema, C.S. Karthik, S. Sandeep, L. Mallesha, N.S. Alsaiari, M. A. Sridhar, K.M. Katubi, K.M. Abualnaja, N.K. Lokanath, P. Mallu, S. R. Kumaraswamy, Persistent prevalence of non-covalent interaction in pyrimidine containing sulfonamide derivative: A quantum computational analysis, J. Mol. Struct. 1266 (2022) 133378, https://doi.org/10.1016/j.molstruc.2022.133378.
- [45] T.N. Lohith, M.K. Hema, C.S. Karthik, S. Sandeep, L. Mallesha, P. Mallu, R. Jothi Ramalingam, M.A. Sridhar, M. Karnan, N.K. Lokanath, N-[2-(5-bromo-2-chloro-pyrimidin-4-yl)thio)-4-methoxy-phenyl]-4-chlorobenzenesulfonamide: The existence of H-bond and halogen bond interactions assisted supramolecular architecture A quantum chemical investigation, J. Mol. Struct. 1267 (2022) 133476, https://doi.org/10.1016/j.molstruc.2022.133476.
- [46] M. Mehri, N. Chafai, L. Ouksel, K. Benbouguerra, A. Hellal, S. Chafaa, Synthesis, electrochemical and classical evaluation of the antioxidant activity of three α-aminophosphonic acids: experimental and theoretical investigation, J. Mol. Struct. 1171 (2018) 179–189.
- [47] B.S. Chethan, H.R. Rajegowda, D.V. Padmaja, N.K. Lokanath, Synthesis, structural and exploration of non-covalent interactions of the palladium complex with the crystalline water molecule: A comprehensive quantum chemical approach, J. Mol. Struct. 1274 (2023) 134419.
- [48] E.R. Johnson, S. Keinan, P. Mori-Sánchez, J. Contreras-García, A.J. Cohen, W. Yang, Revealing noncovalent interactions, J. Am. Chem. Soc. 132 (2010) 6498–6506.
- [49] D.V. Kumar, S. Kumar, K.N. Murthy, B.M. Rajesh, T.N. Lohith, Ordering self-assembly structures via NH··· S and Br··· S interactions in (E)-2-(4-bromobenzylidene) hydrazinecarbothioamide: insights from crystallographic and computational study, J. Mol. Struct. (2024) 138285.
- [50] D.V. Kumar, B.S. Chethan, D. Gowda, K.S. Rangappa, N.K. Lokanath, Investigation of the crystal structure, supramolecular architecture and in-silico myelofibrosis

- inhibition of a triazole derivative: a structural and theoretical approach, J. Mol. Struct. 1288 (2023) 135770.

 [51] D.V. Kumar, B.S. Chethan, V. Shalini, K.S. Rangappa, N.K. Lokanath, Structural elucidation and in-silico evaluation of 1, 2, 4-triazole derivative as potent Omicron

- variant of SARS-CoV-2 spike protein inhibitor with pharmacokinetics ADMET and drug-likeness predictions, J. Mol. Struct. 1297 (2024) 136976.

 [52] C.A. Lipinski, F. Lombardo, B.W. Dominy, P.J. Feeney, Experimental and computational approaches to estimate solubility and permeability in drug discovery and development settings, Adv. Drug Deliv. Rev. 23 (1997) 3–25.